International Journal of Mechanical Sciences 148 (2018) 352–365

Contents lists available at ScienceDirect

International Journal of Mechanical Sciences

journal homepage: www.elsevier.com/locate/ijmecsci

Hydrodynamic characteristics of an inclined slender flexible cylinder subjected to vortex-induced vibration

Qinghua Han[a,b,c], Yexuan Ma[a,c], Wanhai Xu[a,b,*], Dixia Fan[d], Enhao Wang[a]

[a] State Key Laboratory of Hydraulic Engineering Simulation and Safety, Tianjin University, Tianjin 300072, China
[b] Collaborative Innovation Centre for Advanced Ship and Deep-Sea Exploration, Shanghai 200240, China
[c] School of Civil Engineering, Tianjin University, Tianjin 300072, China
[d] Department of Mechanical Engineering, Massachusetts Institute of Technology, Cambridge MA02139, USA

ARTICLE INFO

Keywords:
Inclined flexible cylinder
Vortex-induced vibration (VIV)
Lift coefficient
Drag coefficient
Added mass coefficient

ABSTRACT

The hydrodynamic coefficients (e.g., lift coefficients, drag coefficients and added mass coefficients) are key parameters for predicting the vortex-induced vibration (VIV) of flexible cylinders. It is an experimental challenge to directly measure the forces/coefficients along a flexible cylinder during model tests without disturbing the flow field. However, such hydrodynamic features can be successfully obtained via an inverse analysis of the displacement responses based on the structural dynamics. In this paper, the hydrodynamic coefficients were calculated using the towing tank experimental results of an inclined flexible cylinder undergoing VIV at five different inclination angles ($\alpha = 0^\circ$, 15°, 30°, 45° and 60°, where α denotes the inclination angle defined as the angle between the cylinder axis and the plane orthogonal to the oncoming fluid flow). It is found that the influence of the inclination angle on the hydrodynamic coefficients is generally insignificant when the inclination angle is varied from 0° to 15°. In contrast, the hydrodynamic characteristics of the inclined cylinder with large inclination angles ($\alpha = 45^\circ$ and 60°) are distinct from those of the vertical flexible cylinder ($\alpha = 0^\circ$) and this difference becomes more evident as the inclination angle is increased. The RMS of the fluctuating force coefficients in the cross-flow (CF) and in-line (IL) directions, mean drag coefficients, axial mean lift and varying drag coefficients in the case of $\alpha = 60^\circ$ are much larger than those in the normal case($\alpha = 0^\circ$). Meanwhile, the axial mean IL added mass coefficients in the cases of $\alpha = 45^\circ$ and 60° demonstrate higher values compared to those in the normal case at certain reduced velocities. It can be speculated that different wake behaviors are associated with the distinct hydrodynamic behaviors of the inclined flexible cylinder at different inclination angles. Within the same mode synchronized region, the axial distributions of the hydrodynamic coefficients in the cases of $\alpha = 15^\circ$ and 30° resemble that of the vertical flexible cylinder, while the spanwise variations of the hydrodynamic coefficients for $\alpha = 45^\circ$ and 60° agree well with each other.

1. Introduction

Alternating vortex shedding behind a bluff body could lead to vortex-induced vibration (VIV) if the structure is free to oscillate in cross-flow (CF) direction only or in both CF and in-line (IL) directions. VIV is a ubiquitous natural phenomenon, especially for slender cylindrical objects. It may result in severe fatigue damage if not dealt with properly. Hence, it has become one of the most challenging issues in many fields of engineering. A large number of research works have been devoted to this complex fluid-structure interaction (FSI) problem from many perspectives, including wake flow behaviors, FSI mechanisms, structural responses and hydrodynamic features [1–5].

The fluctuating forces in the CF and IL directions, which give rise to VIV, are caused by the alternatively shed vortices around the cylinder. If the cylinder is fixed in the flow, the fluctuating forces do not contain the added mass forces and are named as lift and drag in the CF and IL directions, respectively. The drag can be further divided into the varying drag and the mean drag [6]. In order to enhance our understanding of VIV, the hydrodynamic characteristics of the flow around a fixed cylinder have been studied extensively over the past several decades [7]. If the cylinder is allowed to vibrate in the flow, the CF fluctuating forces can be decomposed into one part in phase with the velocity, and the other in phase with the acceleration, namely the lift and CF added mass force [8]. Similarly, the IL fluctuating forces consist of the varying drag and IL added mass force [9].

There have been many publications on the hydrodynamics of an elastically-mounted rigid cylinder subjected to forced or free vibrations

* Corresponding author at: State Key Laboratory of Hydraulic Engineering Simulation and Safety, Tianjin University, Tianjin 300072, China.
E-mail address: xuwanhai@tju.edu.cn (W. Xu).

https://doi.org/10.1016/j.ijmecsci.2018.09.010
Received 17 March 2018; Received in revised form 5 September 2018; Accepted 6 September 2018
Available online 7 September 2018
0020-7403/

in fluid flow [8–13]. The mean drag coefficients increase with increasing CF displacements and reach the highest point as "lock-in" occurs. Moreover, the CF fluctuating force coefficients soar to the maximum value within the "lock-in" region and are followed by a slump. The drop is closely related to the jump of the phase between the lift coefficients and CF displacements, attributed to the switch of near wake patterns [10]. The lift coefficients show a significant dependence on the response amplitudes and frequencies of the structure and would peak when the vortex shedding frequency synchronizes with the natural frequency [8,13]. The magnitudes of the varying drag coefficients are small at low amplitudes and frequencies, whereas they rocket to prominent values when the amplitudes and frequencies reach high values [9]. The added mass coefficients are proved to be more relevant to the response frequency than the response amplitude within "lock-in" region [11,12].

The hydrodynamic coefficients of elastically-mounted rigid cylinders undergoing forced vibrations have been employed in the empirical models for predicting the VIV responses of flexible cylinders, such as VIVA, VIVANA, VICoMo, SHEAR7 and ABAVIV. However, there exist considerable discrepancies between the VIV prediction results and experimental results [14]. Utilizing VIV hydrodynamic coefficients of long flexible cylinders could further improve the prediction accuracy. Unfortunately, it is difficult to measure the hydrodynamic forces acting along the flexible cylinders directly during model tests without affecting the ambient flow field. Previous researchers applied indirect methods to identify the fluid forces [15–18]. Huera-Huarte [15] proposed a finite element method (FEM) to calculate the fluid forces of a flexible cylinder undergoing VIV based on the displacement responses. It was found that the axial distributions of the fluctuating forces and displacements in the CF direction followed an analogous trend. Tang et al. [16] employed the master-slaved technique to reduce all the rotational degrees of freedom and input the VIV displacements into a finite element model to obtain the fluid forces. It was pointed out that the lift and varying drag coefficients were associated with the energy transfer. Song et al. [17] acquired the hydrodynamic forces on a flexible cylinder by an inverse analysis method. It was found that the hydrodynamic coefficients of a flexible cylinder undergoing VIV disagreed with those obtained from forced oscillation tests of rigid cylinders and the added mass coefficients were dependent on the response frequencies and the response amplitudes. Wu et al. [18] investigated the effect of the phase angles between IL and CF displacements on the lift coefficients. It was concluded that the lift coefficients were associated with the motion phase angles and tended to have a strong spatial variation as the response have a significant contribution of standing waves.

It is well known that cylindrical structures are often inclined with respect to the direction of the oncoming flow in practical engineering applications. The inclination angle α is defined as the angle between the cylinder axis and the plane perpendicular to the oncoming flow. Hence, $\alpha = 0^\circ$ is corresponding to the normal flow configuration. In order to estimate the vortex shedding characteristics of inclined rigid cylinders, Hanson [19] and Van Atta [20] introduced the Independence Principle (IP) which assumes that the wake flow of the inclined cylinders are essentially driven by the inflow normal component and the axial component has a negligible impact. In recent years, the validity of the Independence Principle has been verified by examining the fluid-structure interaction characteristics (e.g. the vortex shedding behaviors, hydrodynamic features and structural responses) of fixed or elastically supported rigid cylinders inclined to the oncoming flow [21–26]. However, the performance of the Independence Principle in predicting VIV hydrodynamic coefficients of the inclined flexible cylinders has been scarcely reported.

The hydrodynamic characteristics of an inclined stationary cylinder are obviously different from those of a cylinder normal to the flow as a result of the three-dimensional flow features [21]. Some experimental and numerical studies on the hydrodynamic behaviors of a fixed cylinder inclined at different inclination angles have been conducted by Ramberg [21] and Zhao et al. [22,23]. The three-dimensional wake vortex flow was observed in the case of flow past an inclined stationary cylinder with finite length. The values of the mean drag coefficients and lift coefficients are much higher than that predicted by the Independence Principle, especially in the case of large inclination angles owing to the strong influence of the axial flow on the vortex shedding. The hydrodynamic force coefficients show strong spanwise dependence due to the significant effect of the three-dimensional phenomenon.

The hydrodynamic mechanisms become more complicated if the inclined cylinder can oscillate in the flow. Several researchers have considered the VIV hydrodynamics of inclined elastically supported rigid cylinders. Lucor and Kamiadakis [24] numerically studied the hydrodynamics of an inclined elastically supported cylinder undergoing VIV with $\alpha = 0^\circ$, $-60^\circ$and -70°. It was found that the base pressures on the inclined cylinder were lower than the results predicted by the Independence Principle, which produced significantly greater drag coefficients than those estimated by the Independence Principle. Franzini et al. [25] conducted model tests to explore the hydrodynamics of an inclined elastically supported rigid cylinder with the CF oscillation only. The inclination angles were set to 0°, $-20^\circ$and -45°, respectively. It was found that the CF fluctuating force coefficients did not decrease significantly as the inclination angle was increased, and the added mass coefficients gradually dropped in "lock-in" region. Franzini et al. [26] carried out experiments on VIV of an inclined rigid cylinder elastically supported in both the CF and IL directions with $\alpha = 0^\circ$, $\pm 15^\circ$, $\pm 30^\circ$ and $\pm 45^\circ$. It was observed that the mean drag coefficients and the CF fluctuating force coefficients reduced at larger inclination angles. However, the mean drag coefficients were positively related to the displacement in the CF direction.

Nevertheless, little attention has been paid to the VIV hydrodynamics of inclined flexible cylinders. Recently, Bourguet et al. [27] and Bourguet and Triantafyllou [28] studied VIV of inclined flexible cylinders at $\alpha = 60^\circ$ and 80° by means of direct numerical simulation (DNS). It was found that the part of the inflow axial component perpendicular to the cylinders could result in distinct responses of the fluid-structure system and affected the hydrodynamic characteristics. The mean drag coefficients and lift coefficients of the inclined cylinder were much higher than those of the vertical cylinder. In addition, there was an obvious discrepancy in the axial distribution of the hydrodynamic coefficients between the inclined cylinder and the vertical one. Han et al. [29] performed experimental investigations of the VIV responses and the mean drag features of an inclined flexible cylinder with $\alpha = 45^\circ$ in uniform flow. The mean drag coefficients were obtained using the FEM technique put forward by Huera-Huarte [15]. It was found that the mean drag coefficients of the inclined flexible cylinder at $\alpha = 45^\circ$ agreed well with those of the vertical cylinder. In addition, the mean drag coefficients of the inclined flexible cylinder did not show a sharp decrease, which was inconsistent with the trend of an inclined rigid cylinder.

According to the aforementioned literature review, the VIV hydrodynamic characteristics of an inclined flexible cylinder differ from those of an inclined rigid cylinder. Hence, the VIV hydrodynamic features of the inclined cylinder urgently need to be further investigated. There are two main objectives of our current research. The first one is to study the effects of the inclination angle on the hydrodynamic characteristics of an inclined flexible cylinder undergoing VIV. The second one is to improve the database of VIV hydrodynamic coefficients to a certain extent. In this paper, the hydrodynamic coefficients are obtained indirectly from the displacement responses from our previous towing tank experimental campaigns on VIV of an inclined flexible cylinder with five inclination angles ($\alpha = 0^\circ$, 15°, 30°,45° and 60°) [30].

The outline of the rest of the paper is as follows. Section 2 introduces the method for force calculations and a brief description of the experimental arrangement and data processing is provided in Section 3. In Section 4, the results of the hydrodynamic coefficients and in-depth discussions about their characteristics varying with the inclination angle are presented. Finally, the conclusions of this paper are summarized in Section 5.

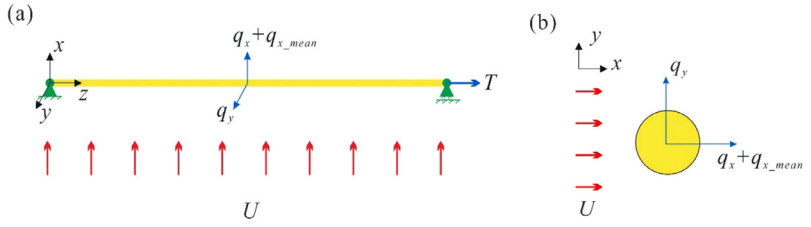

Fig. 1. Schematics of the flexible cylinder model. (a) general view;(b) cross-sectional view.

2. Calculation of the fluid forces of a flexible cylinder undergoing VIV

As we know, it is very challenging to measure the VIV hydrodynamic forces of a flexible cylinder directly and cause negligible effects on the flow field. However, the hydrodynamic forces of a flexible cylinder can be calculated by inverse analysis methods. Such methods for reconstruction of fluid forces have been proved to be feasible [15,17,18]. The response displacements of a flexible cylinder undergoing VIV can be obtained easily from the model test. The flexible cylinder model can be separated into multiple beam elements according to the finite element method. Taking the response displacement as the input data, the hydrodynamic forces are determined inversely from the finite element model of the flexible cylinder. Subsequently, lift coefficient, drag coefficient and added mass coefficient can be obtained by decomposing the hydrodynamic force using the least squared method.

Fig. 1 shows the schematics of the flexible cylinder model. Axis of x denotes the IL direction. Axis of y stands for the CF direction. Axis of z denotes the axial direction of the cylinder. U is the uniform flow velocity. T is the axial tension. q_x and q_y are the IL and CF fluctuating forces, respectively. q_{x_mean} is the mean drag in the IL direction. The flexible cylinder can be modeled as an Euler–Bernoulli beam, and the governing vibration equations in the IL and CF direction are expressed as Eqs. (1) and (2) [17],

$$EI\left(x'''' + x''''_{mean}\right) - T\left(x'' + x''_{mean}\right) + c_x\dot{x} + m_s\ddot{x} = q_x + q_{x\_mean} \tag{1}$$

$$EIy'''' - Ty'' + c_y\dot{y} + m_s\ddot{y} = q_y \tag{2}$$

where EI is the bending stiffness, m_s represents the structural mass per unit length, c_x and c_y are the structural damping coefficients in the IL and CF directions, respectively. x and y are the IL and CF displacements, respectively. A dot denotes differentiation with respect to time. It is noted that the governing equation in the IL direction is different from that in the CF direction. Due to the effect of the uniform flow, the flexible cylinder experience a mean drag q_{x_mean} in the IL direction which causes the mean displacement x_{mean} [17]. x'''', x''''_{mean} and y'''' represent the fourth-order partial derivative with respect to the axial coordinate z. x'', x''_{mean} and y'' indicate the second-order partial derivative with respect to z. As the mean displacement x_{mean} is caused by the mean drag and the IL oscillating displacement x is closely related to the IL fluctuating force q_x, the IL governing equation (1) can be split into Eqs. (3) and (4).

$$EIx''''_{mean} - Tx''_{mean} = q_{x\_mean} \tag{3}$$

$$EIx'''' - Tx'' + c_x\dot{x} + m_s\ddot{x} = q_x \tag{4}$$

The fluid forces acting on the flexible cylinder can be identified by a finite element method [15,16,18]. The flexible cylinder model is idealized as an assembly of the beam elements. There are four degrees of freedom (DOF) in each element, namely two translation and two rotation DOFs at the end of the element. Eqs. (2)–(4) are rearranged into the following finite element form,

$$(K_E + K_P)X_{mean} = Q_{x\_mean} \tag{5}$$

$$M_s\ddot{X} + C_X\dot{X} + (K_E + K_P)X = Q_x \tag{6}$$

$$M_s\ddot{Y} + C_Y\dot{Y} + (K_E + K_P)Y = Q_y \tag{7}$$

where M_s is the mass matrix, K_E represents the elastic stiffness matrix, K_P denotes the geometric matrix. X and Y are the vectors of IL and CF oscillating displacements, respectively. Q_x, Q_{x_mean} and Q_y are the fluid load matrices. C_X and C_Y are the structural damping matrices. Taking the structural damping in the CF direction as an example, the structural damping matrix C_Y can be expressed as Rayleigh damping form [15,16],

$$C_Y = \lambda_1 M_s + \lambda_2(K_E + K_P) \tag{8}$$

where λ_1 and λ_2 can be calculated using any two of the modal damping ratios and the natural circular frequency of the corresponding modes [15].

$$\begin{cases} \dfrac{\lambda_1 + \lambda_2{\omega_k}^2}{2\omega_k} = \xi_k \\ \dfrac{\lambda_1 + \lambda_2{\omega_p}^2}{2\omega_p} = \xi_p \end{cases} \tag{9}$$

According to Eq. (9), we can obtain λ_1 and λ_2. ω_k and ω_p are the k-, p-order natural circular frequencies, respectively. ξ_k and ξ_p are the k-, p-order structural damping ratios, respectively. The flexible cylinder has multi-order natural frequencies, which can be obtained by theoretical calculation or free decay tests in air [15].

q_x, q_{x_mean} and q_y can be obtained from the fluid load matrices if Q_x, Q_{x_mean} and Q_y are calculated according to Eqs. (5)–(7). The root-mean-square (RMS) of the IL and CF fluctuating force coefficients can be acquired by Eqs. (10) and (11).

$$C_{IL\_rms} = \frac{2}{\rho DU^2 l}\left(\frac{l}{L}\sum_{i=1}^{L/l}\sqrt{\frac{1}{N_s}\sum_{j=1}^{N_s}{q_x}^2(z_i,t_j)}\right) \tag{10}$$

$$C_{CF\_rms} = \frac{2}{\rho DU^2 l}\left(\frac{l}{L}\sum_{i=1}^{L/l}\sqrt{\frac{1}{N_s}\sum_{j=1}^{N_s}{q_y}^2(z_i,t_j)}\right) \tag{11}$$

Where N_s is the sampling number. L is the length of the flexible cylinder. l is the element length of the flexible cylinder. ρ is the fluid density. D is the diameter of the cylinder. The mean drag coefficients C_{D0} can be calculated from Eq. (12).

$$C_{D_0} = \frac{2}{\rho DU^2 l}\left(\frac{l}{L}\sum_{i=1}^{L/l}q_{x\_mean}(z_i)\right) \tag{12}$$

For an oscillating cylinder, the CF fluctuating force includes not only lift but also added mass force. It can be decomposed into two components, namely lift and CF added mass force. The lift is in phase with velocity and denotes the energy transfer between the structure and fluid. The added mass force is in phase with acceleration and determines the added mass coefficient. Similarly, the IL fluctuating force can be decomposed into varying drag and IL added mass force [8,9,17]. The forces q_x

and q_y obtained from the inverse analysis method are regarded as the real fluid forces. While $q_{x\_predict}$ and $q_{y\_predict}$ represent the predicted values of the vortex shedding forces. The predicted fluid forces $q_{x\_predict}$ and $q_{y\_predict}$ can be presented as follows [17],

$$q_{x\_predict} = \frac{\rho Dl}{2\sqrt{2}\dot{x}_{rms}} U^2 C_D \dot{x} - \frac{1}{4}\rho\pi D^2 l C_{ax}\ddot{x} \tag{13}$$

$$q_{y\_predict} = \frac{\rho Dl}{2\sqrt{2}\dot{y}_{rms}} U^2 C_L \dot{y} - \frac{1}{4}\rho\pi D^2 l C_{ay}\ddot{y} \tag{14}$$

The least square method is employed to assure the minimum squared errors of the IL and CF fluctuating forces between the real and predicted values [9,17]. The squared errors can be expressed as [17],

$$e_x{}^2 = \sum_1^{N_s}\left(\frac{\rho Dl}{2\sqrt{2}\dot{x}_{rms}} U^2 C_D \dot{x} - \frac{1}{4}\rho\pi D^2 l C_{ax}\ddot{x} - q_x\right)^2 \tag{15}$$

$$e_y{}^2 = \sum_1^{N_s}\left(\frac{\rho Dl}{2\sqrt{2}\dot{y}_{rms}} U^2 C_L \dot{y} - \frac{1}{4}\rho\pi D^2 l C_{ay}\ddot{y} - q_y\right)^2 \tag{16}$$

The varying drag coefficient C_D, lift coefficient C_L, and IL and CF added mass coefficient C_{ax}, C_{ay} are acquired by finding the minimum $e_x{}^2$ and $e_y{}^2$. The detailed formulas are as follows [17],

$$C_D = \frac{2\sqrt{2}\dot{x}_{rms}}{\rho Dl U^2}\frac{(J_2J_5 - J_3J_4)}{(J_2{}^2 - J_1J_4)} \tag{17}$$

$$C_{ax} = \frac{4}{\pi\rho D^2 l}\frac{(J_1J_5 - J_2J_3)}{(J_2{}^2 - J_1J_4)} \tag{18}$$

$$C_L = \frac{2\sqrt{2}\dot{y}_{rms}}{\rho Dl U^2}\frac{(S_2S_5 - S_3S_4)}{(S_2{}^2 - S_1S_4)} \tag{19}$$

$$C_{ay} = \frac{4}{\pi\rho D^2 l}\frac{(S_1S_5 - S_2S_3)}{(S_2{}^2 - S_1S_4)} \tag{20}$$

where $J_1 = \sum_1^{N_s}\dot{x}^2, J_2 = \sum_1^{N_s}\dot{x}\cdot\ddot{x}, J_3 = \sum_1^{N_s} q_x\cdot\dot{x},\ J_4 = \sum_1^{N_s}\ddot{x}^2, J_5 = \sum_1^{N_s} q_x\cdot\ddot{x}, S_1 = \sum_1^{N_s}\dot{y}^2, S_2 = \sum_1^{N_s}\dot{y}\cdot\ddot{y}, S_3 = \sum_1^{N_s} q_y\cdot\dot{y},\ S_4 = \sum_1^{N_s}\ddot{y}^2, S_5 = \sum_1^{N_s} q_y\cdot\ddot{y}$. $\dot{x}_{rms}$ and $\dot{y}_{rms}$ denote the RMS of IL and CF velocities, respectively.

When we use the aforementioned method to calculate the hydrodynamic force coefficients of inclined flexible cylinders, the flow velocity U should be replaced by equivalent velocity U_n. The equivalent velocity U_n is equal to $Ucosa$, which is the component of flow velocity vertical to the cylinder axis. In this way, it is convenient to compare the various results at different inclination angles.

3. Description of the model tests

To the best knowledge of the authors, there are very few available experimental results of inclined flexible cylinder undergoing VIV. More recently, Xu et al. [30] carried out a series of laboratory tests on the VIV of an inclined flexible cylinder in a towing tank to investigate the effects of inclination angle on the VIV dynamic characteristics. In this paper, the VIV hydrodynamic force coefficients of an inclined flexible cylinder are obtained based on the results of displacement responses in Xu et al. [30].

3.1. Experimental arrangement

A brief introduction to the model tests is presented in this section. The readers are referred to Xu et al. [30] for more details about the experiments. Fig. 2 shows the sketch of the experimental apparatus. One end of the cylinder model was connected to a universal joint fixed on the supporting plate. The other end of the flexible cylinder model was connected to a steel wire, which was passed through a pulley and connected to the spring, tensioner and load cell in sequence. The application of spring allowed a gradual variation of the axial tension on the cylinder model during the tests. The tensioner was used to adjust the axial tension to 300 N for all the cases. The load cell was adopted to monitor the axial tension.

Table 1
Geometric and mechanical parameters of the cylinder model.

Parameters	Values
Total length, L	5.60 m
Outer diameter, D	0.016 m
Bending stiffness, EI	17.45 Nm^2
Axial tension, T	300 N
Mass per unit length, m_s	0.3821 kg/m
Mass ratio, m^*	1.90
Aspect ratio, L/D	350

Five inclination angles, $a = 0°$, 15°, 30°, 45° and 60°, were selected by adjusting the angle on the angle plate which is shown in Fig. 3. The supporting plate could be rotated with the rotation of the angle plate. Moreover, it should be pointed out that the plane of the supporting plate must always keep parallel with the flow direction. The horizontal supporting frame was connected to the towing carriage with an inclination angle which was same as the setting of the angle plate, ensuring the cylinder model inclined at a corresponding angle. The test schematics is shown in Fig. 4.

The flexible cylinder model used in the tests was a coaxial composite tube. The inner part of the cylinder was a copper pipe with seven measurement points, G1-G7, evenly distributed along the axial direction. A total of 28 resistance strain gauges were instrumented on the surface of the copper pipe in both the CF and IL directions to collect the information of bending strains by half-bridge topology. The outer part of the cylinder model was a silicon tube which not only provided a smooth external surface but also protected and insulated the measuring instrumentation. The key parameters of the cylinder model are listed in Table 1.

The flexible cylinder model was submerged 1.0 m below the free surface to avoid its effect. The uniform flow was generated by towing the cylinder model in still water from 0.05 m/s to 1.0 m/s with an interval of 0.05 m/s. The sampling time was 50 s. The sampling frequency was 100 Hz, which is enough to prevent aliasing problems. The interval between two consecutive runs was at least 15 min, eliminating the water disturbance before a new run.

3.2. Natural frequencies and structural damping

As shown in Eq. (9), the constant coefficients of Rayleigh damping λ_1 and λ_2, are calculated according to the structural damping ratios and the natural circular frequencies, which can be obtained from the free decay tests in air. A hammer was applied to hit the flexible cylinder to excite the oscillations in the CF and IL directions, respectively. The flexible cylinder has multi-order natural frequencies, and multi-mode vibration can be induced due to the sudden impact. The free decay curve can be decomposed into time histories of the responses at different modes by modal decomposition. The structural damping ratio and the natural frequency at different modes can be calculated.

As a typical example, Fig. 5 shows the time history and amplitude spectrum of CF strains of the inclined cylinder with $a = 45°$ at the 1st mode. The structural damping ratio is determined from the following expression,

$$\xi_1 = \frac{1}{2\pi s}\ln\frac{A_1}{A_{s+1}} \tag{21}$$

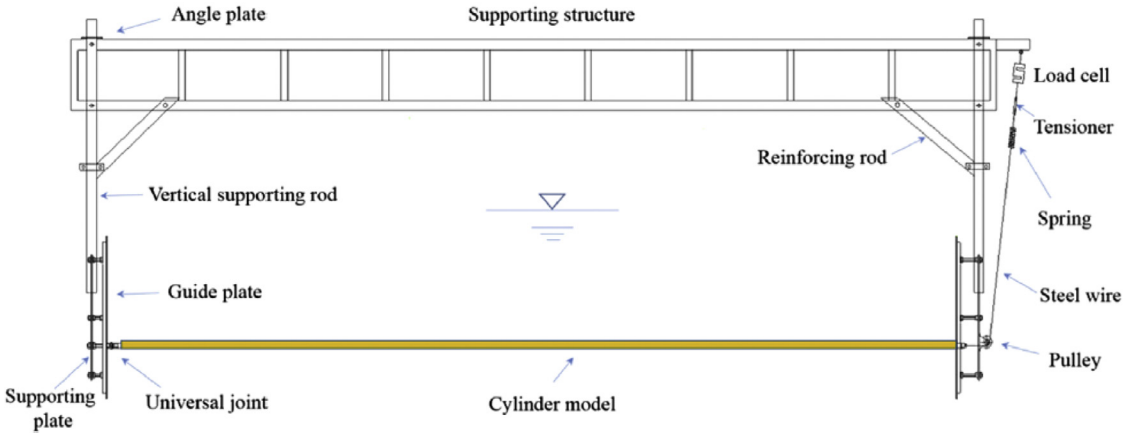

Fig. 2. Sketch of the experimental apparatus [30].

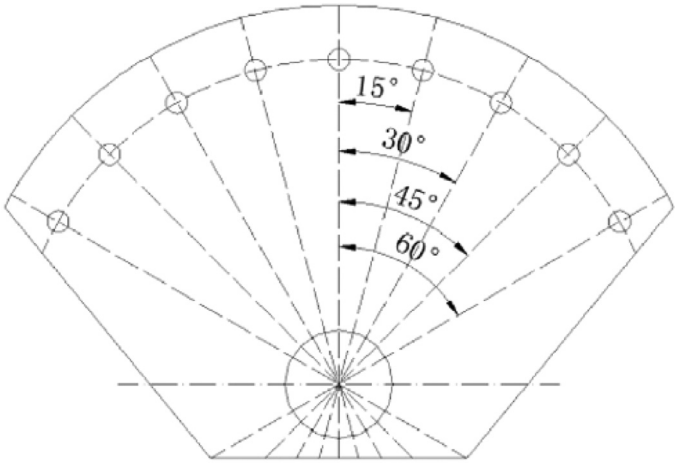

Fig. 3. Angle plate.

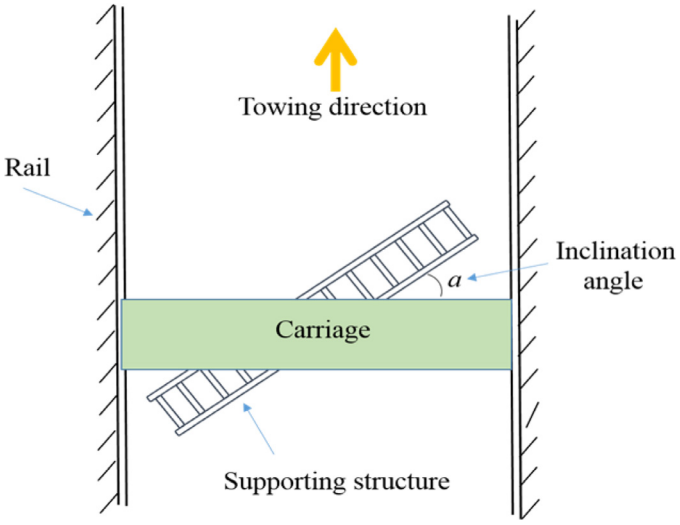

Fig. 4. Test schematics.

where A_1 and A_{s+1} are peak values of the strains, s is the number of cycles between the first and the $(s+1)$th cycle. The natural frequency can be acquired by the fast Fourier transform (FFT) using the time-varying strain signals. As shown in Fig. 5b, the 1st natural frequency in air is 2.80 Hz in this example. It is well known that the natural circular frequency is equal to natural frequency multiplied by 2π. The structural damping ratios and natural frequencies at other modes can be calculated in a similar way.

Free decay tests in water were also conducted. The natural frequencies were compared with the analytical values which were calculated as follows [30],

$$f_n = \frac{n}{2L}\sqrt{\frac{T}{m} + \left(\frac{n\pi}{L}\right)^2 \frac{EI}{m}} \tag{22}$$

where f_n is the nth natural frequency of the cylinder, m is the mass per unit length, including the structural mass and added mass which can be estimated by $\rho\pi D^2/4$. The experimental results of the natural frequencies in water agree quite well with the analytical results using Eq. (22). The average error is less than 6%, indicating the reliability of

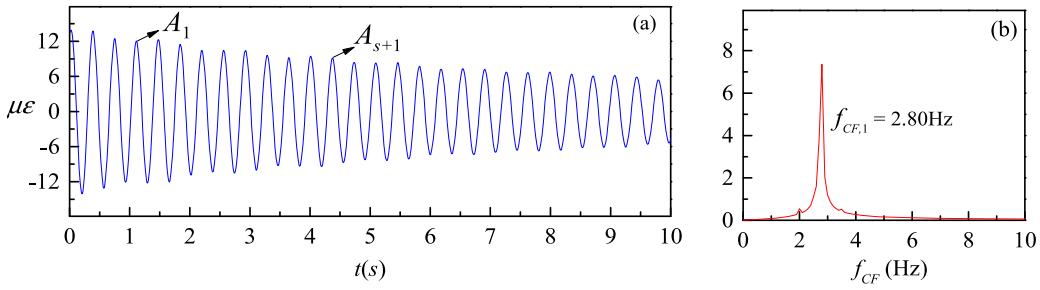

Fig. 5. Time history (a) and amplitude spectrum (b) of CF strain of the inclined flexible cylinder with $a = 45°$ at the midpoint during free decay test in air.

the whole experimental system featured with varying inclination angles of the flexible cylinder [30].

3.3. Displacement reconstruction

Bending strain signals of the flexible cylinder were directly measured in Xu et al. [30], and a modal analysis approach [31] was employed to reconstruct the IL and CF oscillating displacements. Taking the reconstruction of the CF oscillating displacement as an example, the displacement y (z, t) can be composed in the following form,

$$y(z,t) = \sum_{n=1}^{\infty} w_n(t)\varphi_n(z), \qquad z \in [0, L] \tag{23}$$

where t denotes time, $w_n(t)$ is the modal weight, $\varphi_n(z)$ is the mode shape, n is the mode number. The mode shape could be assumed to be sinusoidal or approximated with sinusoids for a pinned-pinned cylinder, as shown in Eq. (24).

$$\varphi_n(z) = \sin\frac{n\pi z}{L} \tag{24}$$

The relationship between the strain ε_y (z, t) and y(z, t) is as follows,

$$\frac{\varepsilon_y(z,t)}{R} = y''(z,t) = -\sum_{n=1}^{N}\left(\frac{n\pi}{L}\right)^2 w_n(t)\sin\frac{n\pi z}{L} \tag{25}$$

where N is the highest mode number participating in the CF direction. As mentioned in Section 3.1, the strain gauges were attached to the outer surface of the copper pipe and the bending stiffness of the silicon tube can be neglected. Hence, R is the radius of the copper pipe. According to Eq. (25), the modal weight w_n(t) can be calculated based on the strains at the measurement points. Substituting the modal weight into Eq. (23), the CF oscillating displacement was obtained.

The IL mean displacement x_{mean} can be expressed in terms of the strains induced by the initial bending ε_{x_mean}(z) [17].

$$x''_{mean}(z) = \frac{\varepsilon_{x\_mean}(z)}{R} \tag{26}$$

From Eq. (26) the IL mean displacement x_{mean} was calculated.

4. Hydrodynamic characteristics of the inclined flexible cylinder

The VIV hydrodynamic coefficients of the inclined flexible cylinder are presented in this section. It is noted that the reduced velocity V_r in this paper is equal to $U\cos(a)/f_1D$. Herein, f_1 is the 1st natural frequency of the flexible cylinder calculated from Eq. (22).

4.1. CF and IL fluctuating force coefficients

Fig. 6 shows the RMS of the CF fluctuating coefficients versus the reduced velocity. The IL and CF fluctuating force coefficients shown in Figs. 6 and 7 are calculated according to Eqs. (10) and (11). The experimental results of elastically supported rigid cylinders [10,26] and flexible cylinders [15,32] are presented in Fig. 6. As the VIV oscillation amplitudes in the CF direction are insignificant at $V_r \le 2.0$, the calculated hydrodynamic coefficients are erroneous at those reduced velocities and thus not presented. It can be seen that the RMS of the CF fluctuating coefficients of the vertical flexible cylinder peaks at the 1st mode resonance and then decreases before the vibration enters into the 2nd dominant mode, which is consistent with the variation of C_{CF_rms} of elastically supported rigid cylinders within the "lock-in" region [10,26]. As a series of axial forces were applied during the model tests conducted by Huera-Huarte [15], the RMS of the CF fluctuating force coefficient in his research is much scattered. The vertical flexible cylinder in Huera-Huarte [15] experienced prominent C_{CF_rms} compared to that in the present research, which is mainly attributed to the different flow conditions (i.e., the flexible cylinder oscillated freely in stepped flow in his research). It is noted that the VIV of a flexible cylinder in Sanaati and Kato [32] is tension dominated string-like vibration. Hence, the RMS of the CF fluctuating force coefficients in Sanaati and Kato [32] are similar to that of elastically supported rigid cylinders and smaller than those of the vertical flexible cylinder in this paper as $V_r \ge 10.7$.

It can be seen that the RMS of the CF fluctuating force coefficient of the inclined flexible cylinder at $a = 15^\circ$ is close to that of the vertical flexible cylinder. As the inclination angle is increased to 30°, the C_{CF_rms} is larger than that of the vertical flexible cylinder at the 1st mode resonance. When the reduced velocity is in the range of $V_r \ge 11.9$, the C_{CF_rms} of the inclined flexible cylinder at $a = 30^\circ$ shows a slight discrepancy from that of the vertical flexible cylinder. For $a = 45^\circ$, the flexible cylinder has relatively higher C_{CF_rms} than the cases of $a = 0^\circ$, 15° and 30° at both the 1st and 2nd mode resonance. When $V_r \ge 11.9$, the CF fluctuating force coefficient in the case of $a = 45^\circ$ is close to that of the vertical flexible cylinder. The C_{CF_rms} of the inclined flexible cylinder at $a = 60^\circ$ agrees well with that in the case of $a = 45^\circ$ at the 1st mode resonance. However, the C_{CF_rms} for $a = 60^\circ$ is much larger than that in other cases at $V_r \ge 9.2$. The effects of inclination angle on the CF fluctuating force coefficients of the inclined flexible cylinder is not the same as those on the inclined rigid cylinder. As shown in Fig. 6, the results by Franzini et al [26] suggested that the increase of the inclination angle led to a sharp drop of the RMS of CF fluctuating coefficient on the rigid cylinder. However, the RMS of the CF fluctuating force coefficient of the inclined flexible cylinder does not reduce comparing to that in the normal case at the 1st mode resonance. It is possible that the decline of response amplitudes in the CF direction is responsible for the reduction of the CF fluctuating force coefficient in Franzini et al [26]. Huera-Huarte et al. [36] pointed out that the CF fluctuating force coefficients are positively correlated with the CF displacements within "lock-in" region. Xu et al. [30] also found that there was a slight upward trend for the peak of the RMS displacement with increasing inclination angle, which is inconsistent with the results of the inclined rigid cylinder [26]. It is supposed that this difference can be attributed to two reasons [30]:(1) the flexible cylinder model was used in the experiment of Xu et al. [30] instead of a rigid one; (2) the boundary conditions in the experimental set-up of Franzini et al. [26] were asymmetric. As the consequence of the slight enlargement of the CF displacement of the inclined flexible cylinder with the increase in the inclination angle, the C_{CF_rms} rises correspondingly. Bourguet et al. [27] numerically found that the CF fluctuating force coefficient of the inclined flexible cylinder at $a = 60^\circ$ was much larger than that of the vertical one, which might be caused by the fact that part of the axial component of the inflow is locally perpendicular to the cylinder as the IL bending is large [27]. It can be concluded that the Independence Principle is not applicable to the prediction of the CF fluctuating force coefficients when the inclination angle exceeds 15°. The gap of C_{CF_rms} between the inclined flexible cylinder and the vertical one grows wider with the increase of the inclination angle.

Fig. 7 presents the RMS of the IL fluctuating force coefficient of the inclined flexible cylinder. The experimental results of vertical cylinders by Jauvtis and Williamson [10] and Sanaati and Kato [32] are also included in Fig. 7 for comparison. It is clear that the C_{IL_rms} of an elastically supported rigid cylinder in Jauvtis and Williamson [10] is distinct from that of a flexible cylinder in Sanaati and Kato [32]. Moreover, the IL fluctuating force coefficient of the current research is also different from that in Sanaati and Kato [32] due to the tension dominated string-like vibration in their tests. It is shown in Xu et al. [30] that the RMS of the IL amplitudes is much scattered, which can be attributed to the higher mode of vibration. Consequently, the C_{IL_rms} of the flexible cylinder is also disordered. It can be seen from Fig. 7 that the RMS of IL fluctuating force is sensitive to the reduced velocity and may reach the highest points within the mode synchronized region, such as $V_r = 3.1$, 9.2, 12.2, 23.0 and 27.6. The C_{IL_rms} in the cases of $a = 0^\circ$ and 15° share an identical variation trend with V_r, despite the fact that the C_{IL_rms} at $a = 15^\circ$ is much smaller than that in the normal case at $V_r \le 7.4$ and $V_r \ge 17.8$. For $a = 30^\circ$, the variation of the C_{IL_rms} is analogous to that in the normal case with the values of C_{IL_rms} being much lower than

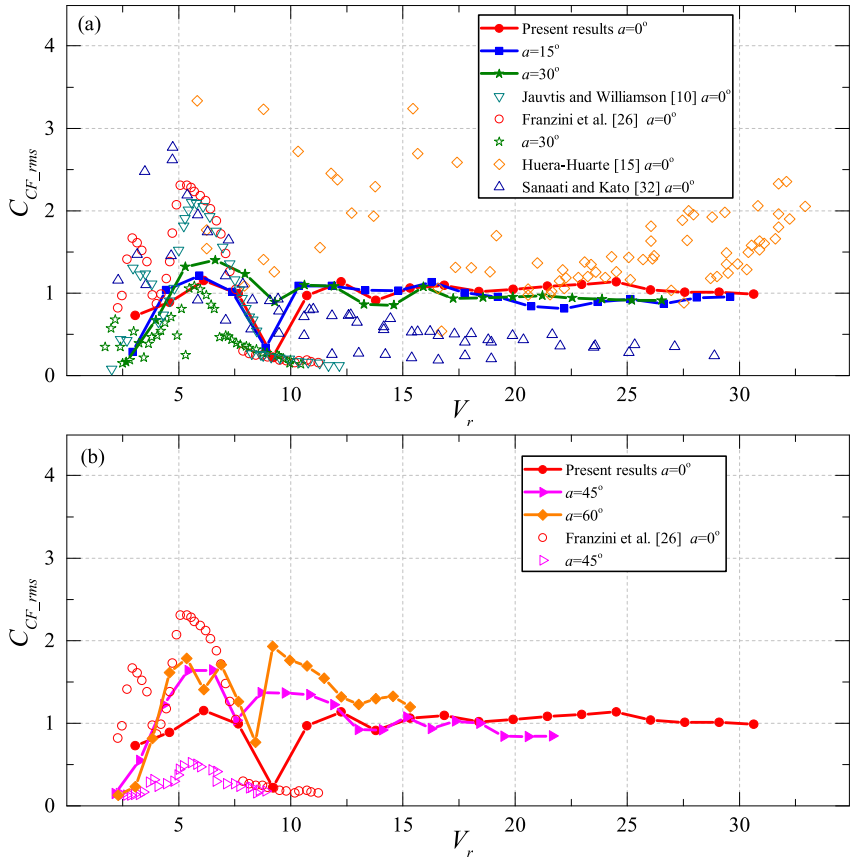

Fig. 6. RMS of the CF fluctuating force coefficients versus the reduced velocity. (a) $\alpha = 0°$, 15° and 30°; (b) $\alpha = 0°$, 45° and 60°.

those of the vertical flexible cylinder at $11.9 \le V_r \le 15.9$ and higher at $18.6 < V_r < 21.2$. A remarkable discrepancy is observed for the RMS of IL fluctuating force coefficient between $\alpha = 45°$ and $\alpha = 0°$, especially at $V_r = 8.4$ and $V_r = 11.9$–18.4, which is closely related to the dominant frequency represented the largest peak in the spectra plot from the FFT analysis of the time-varying displacement. When the inclination angle is increased to 60°, the flexible cylinder experiences extremely prominent C_{IL_rms} compared to that in the other cases, especially at $V_r = 4.6$ and 8.4. It indicates that the inclination angle has a considerable effect on the C_{IL_rms} of an inclined flexible cylinder and the IP cannot predict the C_{IL_rms} accurately even when the flexible cylinder is inclined at a small inclination angle of 15°.

4.2. Mean drag coefficients

The mean drag coefficients of the flexible cylinders are very important parameters for the engineering structure design. Fig. 8 shows the mean drag coefficient of cylinders undergoing VIV which are acquired from Eq. (12) versus the reduced velocity. It is worth noting that the mean drag coefficients always reach the maximum values within the "lock-in" regions. This phenomenon has been observed for vertical cylinders as a consequence of a sudden increase of the response amplitude in the CF direction when the natural frequency of the body and the vortex shedding frequency are synchronized [10,15,26]. The mean drag coefficients of the vertical flexible cylinder agree with the experimental results of other researchers [15]. The results of an inclined elastically supported rigid cylinder [26] showed that the mean drag coefficient decreased with the increase of the inclination angle. However, the C_{D0} of an inclined flexible cylinder does not show a decline when the inclination angle is increased. On the contrary, there is an increase in the mean drag coefficients for $\alpha = 45°$ and 60°. The axial vortices can be stronger with the increase of inclination angle [23], which is perhaps the reason why C_{D0} in the cases of $\alpha = 45°$ and 60° is greater than that in the normal case. For $\alpha = 60°$, the amplification of the mean drag coefficient is remarkable. A similar trend has also been mentioned in Zhao et al. [23] for a stationary rigid cylinder inclined at 45° and in Bourguet and Triantafyllou [28] for a flexible cylinder undergoing VIV with a larger inclination angle of 80°. The inconsistent relationship between the mean drag coefficient and the inclination angle in different research is mainly attributed to the effect of the end conditions adopted in the experimental and numerical simulation setup. Zhao et al. [23] employed a periodic condition at the boundaries to eliminate the influence of end conditions. However, it is difficult to eliminate the effect of the end conditions in the VIV experiments of an inclined rigid cylinder. Therefore, the experimental results of an inclined rigid cylinder presented in Franzini et al. [26] are different from the present experimental results and the numerical results [23,28]. It is interesting that C_{D0} of the vertical flexible cylinder increases significantly at $V_r = 21.5$ and peaks at $V_r = 24.5$. The peak value of C_{D0} at $V_r = 24.5$ is mainly due to the fact that the vibration of the vertical flexible cylinder is at the 3rd mode resonance and the RMS of CF response displacement reaches the maximum value at $V_r = 24.5$ [30]. However, C_{D0} of the flexible cylinder inclined at $\alpha = 15°$ and 30° varies mildly when the reduced velocity is larger than 15.0. The flow component along the axial direction of the inclined flexible cylinder is enhanced as the incoming flow velocities increase to large values. The effect of the axial flow component results that the mean drag coefficient of the inclined flexible cylinder shows a much weaker relationship with the CF response displacement than that of the vertical flexible cylinder.

The mean drag coefficients (C_{D0}) can be roughly estimated if the CF displacements are known, which is of great importance to the structural design in engineering applications. So, it is well worth studying the

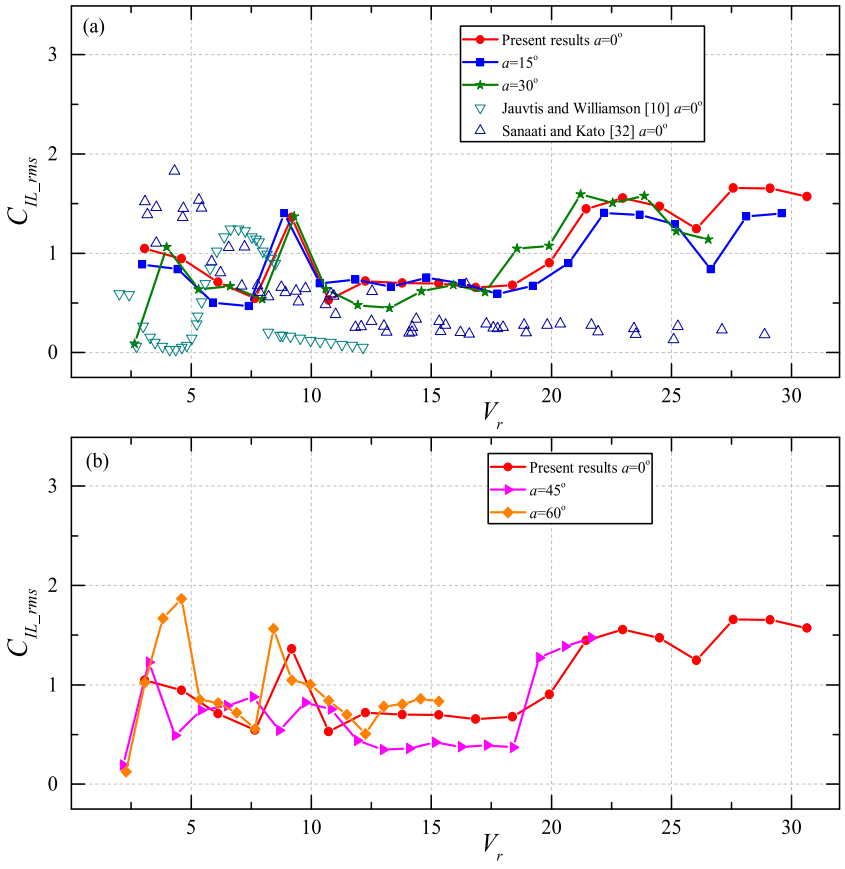

Fig. 7. RMS of the IL fluctuating force coefficients versus the reduced velocity.
(a) $\alpha = 0^\circ$, 15° and 30°; (b) $\alpha = 0^\circ$, 45° and 60°.

correlation between the mean drag coefficients and CF displacements. Fig. 9 presents the mean drag coefficients versus the RMS of CF displacements. The mean drag coefficients of the flexible cylinder have the same growth trend with the increase of CF displacements, as those of the rigid cylinder [10,26]. Vandiver [33] used their field experimental data of long flexible cylinders in steady and uniform flow to obtain an equation which described the relationship between the mean drag coefficients and the CF displacements within "lock-in" condition. This equation can be utilized to predict the mean drag coefficients according to the CF displacements. Song et al. [34] conducted model tests on a flexible cylinder undergoing VIV in the sheared flow. A prediction model for the mean drag coefficients was proposed, considering the dominant mode number, dominant frequency, flow velocity and CF displacement.

A new expression for predicting the mean drag coefficients on an inclined flexible cylinder undergoing VIV at inclination angles ranging from 0° to 60° is proposed according to the expression derived by Vandiver [33] and Song et al. [34], as shown in Eq. (27). The following model for the mean drag coefficient prediction provides a rough guide to the industry.

$$C_{D_0} = C_d\left(1 + \frac{0.17}{\cos^2 a}\left(\frac{2y_{rms}}{D}\right)^{0.65}\right) \tag{27}$$

Where C_d is the mean drag coefficient of a stationary cylinder in water and takes the value of 1.20 in this paper. The trend lines of the mean drag coefficients calculated by Eq. (27) are also plotted in Fig. 9.

4.3. Lift, drag and added mass coefficients

For the sake of analysis, the axial mean values of the lift, drag and added mass coefficients C_{L_mean}, C_{D_mean}, C_{ax_mean} and C_{ay_mean} are presented in this section. The lift, varying drag and added mass coefficients at every node are obtained from Eqs. (17)–(20). Fig. 10 shows the variation of the axial mean lift coefficients with the reduced velocity. It can be seen that the C_{L_mean} of the vertical flexible cylinder ascends to its peak first and then falls consistently within the mode synchronized region. When the higher mode of vibration is excited, the vertical flexible cylinder has preponderant values of the axial mean lift coefficient. For example, the peak of C_{L_mean} of the vertical flexible cylinder is 0.33, 0.78, 0.98 and 1.31 in the first four mode synchronized regions, respectively. The variation of the axial mean lift coefficient in the case of $\alpha = 15^\circ$ is similar to that of the vertical flexible cylinder, which indicates that the inclination angle $\alpha = 15^\circ$ has a negligible influence on the C_{L_mean}. A larger gap of C_{L_mean} between $\alpha = 30^\circ$ and 0° is observed, especially at $V_r = 18.6$ and 19.9. Xu et al. [30] showed that the vibration of the inclined flexible cylinder at $\alpha = 30^\circ$ enters into the 3rd mode synchronized region much earlier than the vertical flexible cylinder, which causes the C_{L_mean} for $\alpha = 30^\circ$ differs from that in the normal case. Remarkable discrepancies of C_{L_mean} are observed between the inclined flexible cylinder and the vertical one when the inclination angle is increased to 45° and 60°. The maximum C_{L_mean} in the case of $\alpha = 45^\circ$ is 0.98 at the 2nd mode resonance, which surpasses the normal case with a value of 0.78. For $\alpha = 60^\circ$, the peak values of axial mean lift coefficients are 0.46 and 1.01 at 1st and 2nd mode resonance, respectively. Both the two values are considerably higher than those of the vertical flexible cylinder.

In this study, some efforts have been taken to figure out why the lift coefficients in the present research are larger than those predicted using the Independence Principle for $\alpha = 45^\circ$ and 60° from the perspective of the wake flow downstream the body. The streamwise and spanwise vortices downstream stationary and oscillating cylinders subject to oblique flow have been investigated experimentally and numerically in some previous publications [21–24,35,36]. Flow visualization results in-

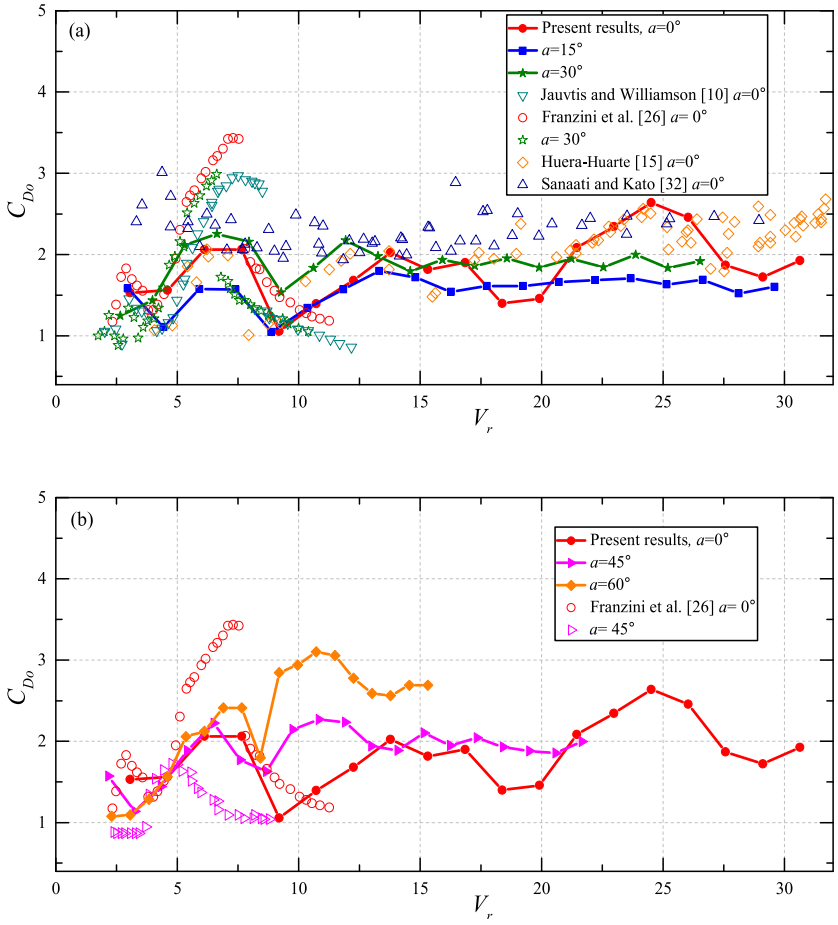

Fig. 8. Mean drag coefficients versus the reduced velocity.
(a) $\alpha = 0^\circ$, 15° and 30°; (b) $\alpha = 0^\circ$, 45° and 60°.

dicated that the spanwise vortices in the wake of a cylinder are oriented at approximately the same angle as the cylinder if $\alpha \leq 45^\circ$. When $\alpha > 45^\circ$, the spanwise vortices are oriented at a smaller angle than the inclination angle [21,24]. For a vibrating cylinder subjected to oblique flow, the critical inclination angle at which the oblique vortex shedding pattern appeared can be delayed. This has already been verified by Lucor and Karniadakis [24], Bourguet et al. [27] and Bourguet and Triantafyllou [28]. The spanwise vortices, parallel to the cylinder axis at $\alpha = 60^\circ$, is slanted when the flexible cylinder is inclined at 80°. Although the parallel vortex shedding downstream an oscillating cylinder subjected to oblique flow is observed, the spanwise vortices exhibit some remarkable characteristics compared to the normal case [27]. Fig. 11 shows the instantaneous iso-surfaces of the spanwise vorticity downstream of the flexible cylinder inclined at $\alpha = 60^\circ$. Fig. 11 was from the numerical investigation on VIV of the inclined flexible cylinder [27]. The flow structures are much more contorted with strong streamwise vortices winding up around the spanwise vortices. This causes that the streamwise vortex tubes are not perpendicular to the cylinder span and they seem to follow helical paths around the spanwise vertical structures. Some of the streamwise vortices are slanted along the direction of the flow and some are slanted along the direction perpendicular to the inflow, indicating the strong influence of the freestream flow direction, which makes the Independence Principle no longer viable [24]. Although the flow patterns downstream the flexible cylinder are unknown in the current investigation, it still can be inferred that the difference between the wake patterns principally accounts for different behaviors of the axial lift coefficient when $\alpha = 45^\circ$ and 60°.

Fig. 12 presents the axial mean varying drag coefficients against the reduced velocity. The C_{D_mean} of the vertical flexible cylinder is scattered due to the complex dynamic behaviors in the IL direction. Fig. 12 demonstrates that the inclination angle has a considerable influence on the C_{D_mean} of the inclined flexible cylinder. The C_{D_mean} at $\alpha = 15^\circ$ is close to that in the normal case when $V_r \leq 10.4$. However, there exist considerable differences when the reduced velocity exceeds 10.0, which may be attributed to the higher mode of vibration in the IL direction. For $\alpha = 30^\circ$, the C_{D_mean} agrees well with that of the vertical flexible cylinder in the range of $8.0 \leq V_r \leq 10.6$. Obvious discrepancies are observed for the rest reduced velocities. The axial mean varying drag coefficient in the case of $\alpha = 45^\circ$ significantly departs from that of the vertical flexible cylinder, especially at $V_r = 8.4$ and $V_r = 11.9$–18.4, where the C_{D_mean} is much lower than that in the normal case. This is mainly due to the fact that the dominant frequency of the displacement is low in such reduced velocity ranges. When the inclination angle equals 60°, the peak value of C_{D_mean} at $V_r = 4.6$ is extremely larger than the C_{D_mean} in the normal case. While the maximum value of C_{D_mean} at $V_r = 8.4$ is slightly smaller than that of the vertical cylinder at $V_r = 9.2$. It can be concluded that the gap of the axial mean varying drag coefficients between the inclined flexible cylinder and the vertical flexible cylinder becomes much wider with the enlargement of the inclination angle due to the aforementioned distinctive wake patterns at different inclination angles.

Figs. 13 and 14 show the variations of the axial mean added mass coefficients with the reduced velocity in the CF and IL directions, respectively. The C_{ay_mean} of the flexible cylinder mildly diminishes as V_r is increased from 2.3 to 7.7, which is in conformity with the results of

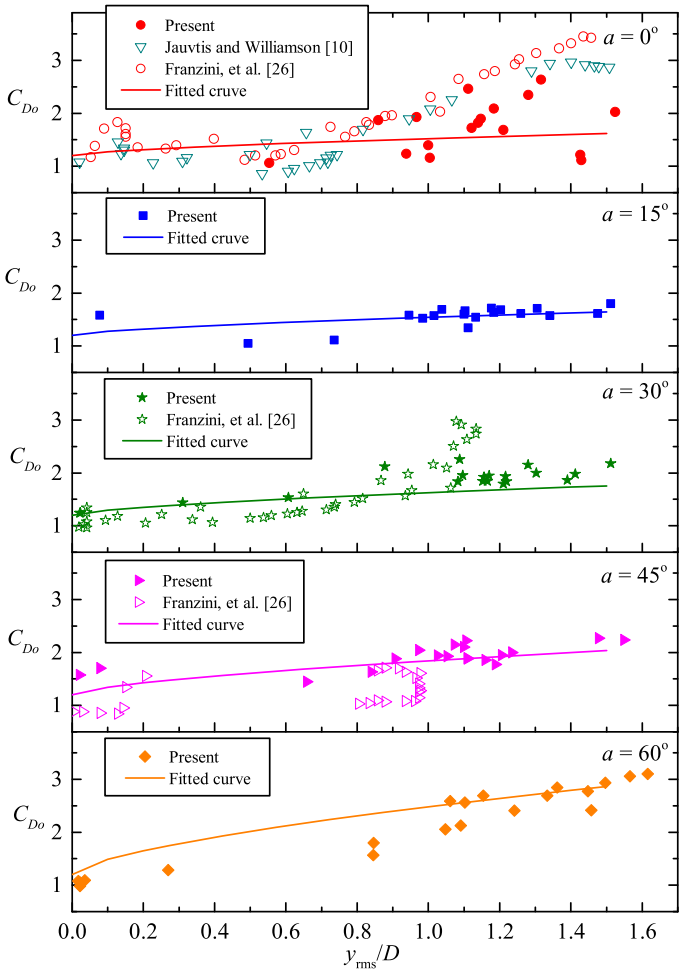

Fig. 9. Mean drag force coefficients versus the max RMS CF dimensionless displacements.

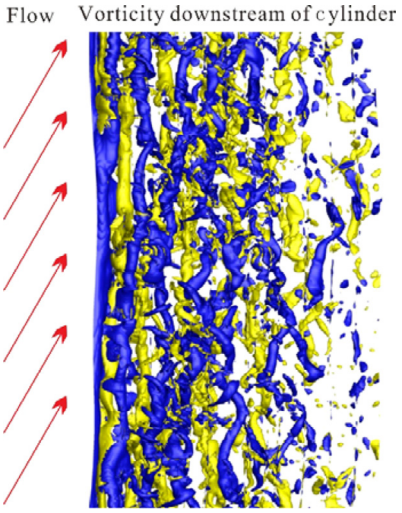

Fig. 11. Instantaneous iso-surfaces of the spanwise vorticity downstream of the flexible cylinder inclined at $a = 60^{\circ}$ [27].

rigid cylinders [8,11,25]. When V_r ranges from 9.0 to 10.0, the C_{ay_mean} jumps abruptly indicating the switch of the dominant mode of vibration in the CF direction from the 1st mode to the 2nd mode. The impact of inclination angles on the CF added mass coefficients is insignificant when $a \leq 45^{\circ}$, whereas the axial mean CF added mass coefficient at $a = 60^{\circ}$ is slightly larger than that in other cases for $V_r \geq 13.8$. Bourguet et al. [27] found that the inclined flexible cylinder at 60° has more prominent CF added mass coefficients than those in the normal case in some regions of the span, which is in accordance with the results of the current research. The axial mean IL added mass coefficients C_{ax_mean} share a similar trend with those in the CF direction, despite the different magnitudes. The vibrations of the inclined flexible cylinder at $a = 30^{\circ}$ and 45° enter the next dominant mode earlier than the vertical flexible cylinder when V_r is roughly in the range of 17.0–20.0 [30]. Thus, C_{ax_mean} of the inclined flexible cylinder at $a = 30^{\circ}$ and 45° is much larger than that of the vertical flexible cylinder. Besides, the inclination angle shows a remarkable influence on C_{ax_mean} for $a = 45^{\circ}$ and 60°. In those cases, the values of C_{ax_mean} are considerably higher than those in the normal case at certain reduced velocities. Similar results have also been reported by Bourguet et al. [27], in which the VIV of an inclined flexible cylinder with $a = 60^{\circ}$ was studied through numerical simulation.

4.4. Axial distribution of hydrodynamic coefficients

For improving the understanding of the VIV hydrodynamic coefficients of an inclined flexible cylinder, the distributions of lift, varying drag and added mass coefficients along the cylinder will be further stud-

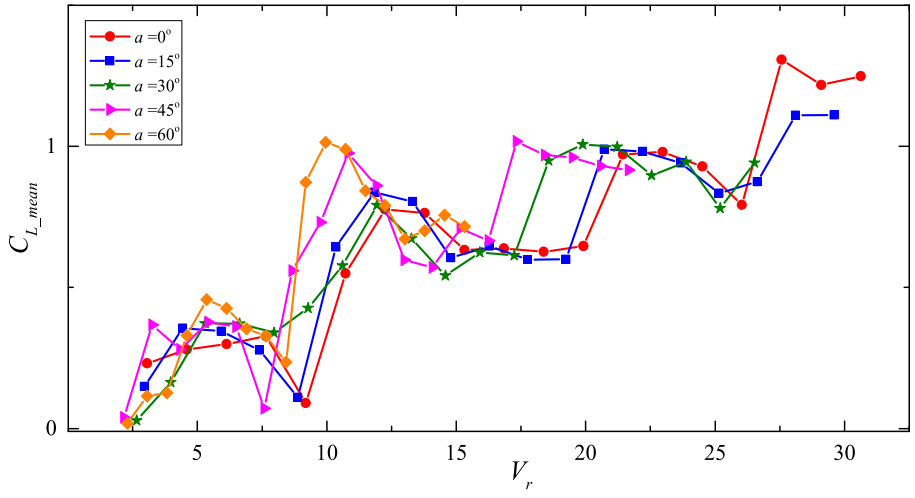

Fig. 10. Axial mean lift coefficients versus the reduced velocity.

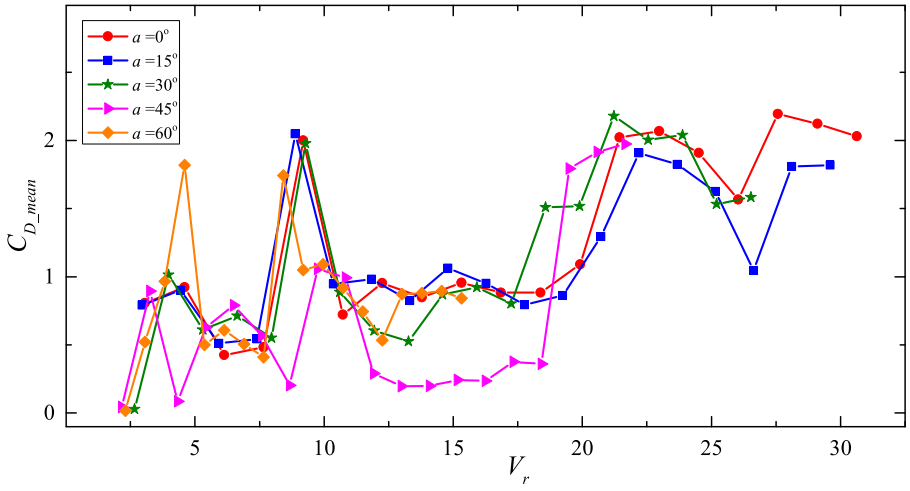

Fig. 12. Axial mean varying drag coefficients versus the reduced velocity.

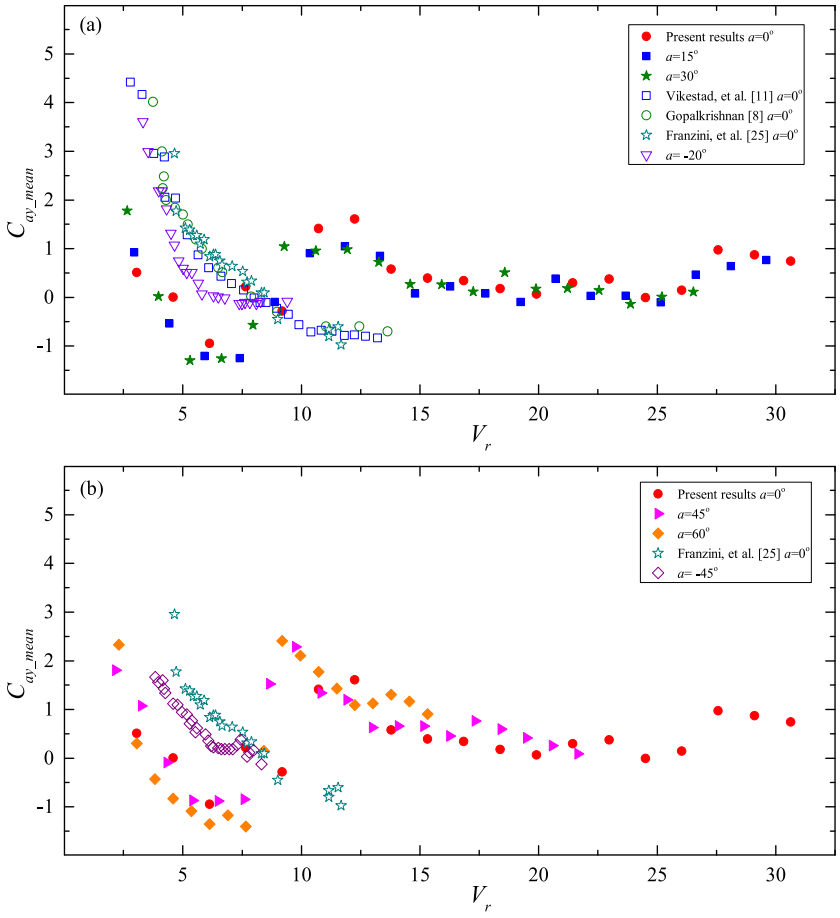

Fig. 13. Axial mean added mass coefficients in the CF direction versus the reduced velocity.
(a) $a = 0°$, 15° and 30°; (b) $a = 0°$, 45° and 60°.

ied in this part. In order to keep this paper reasonably concise, the axial distribution of the hydrodynamic coefficients is not presented for each individual reduced velocity. The results at a reduced velocity of around 10.5 are chosen as an example. According to the results of Xu et al. [30], the vibrations of the flexible cylinder with five inclination angles ($a = 0°$, 15°, 30°, 45° and 60°) are all at the 2nd mode resonance in the CF direction and the 3rd mode resonance in the IL direction at this reduced velocity.

Fig. 15 shows the axial distribution of lift coefficients of the inclined flexible cylinder at the 2nd mode resonance. It is observed that the lift coefficient in the case of $a = 15°$ is in fair agreement with that in the normal case in the ranges of $z/L \leq 0.25$ and $z/L \geq 0.55$. When the inclination angle is increased to 30°, the difference in the lift coefficient between the vertical flexible cylinder and the inclined flexible cylinder becomes more pronounced and quantitative agreement only appears in the range of $z/L \leq 0.38$. The variations of the lift coefficients in the cases of $a = 45°$

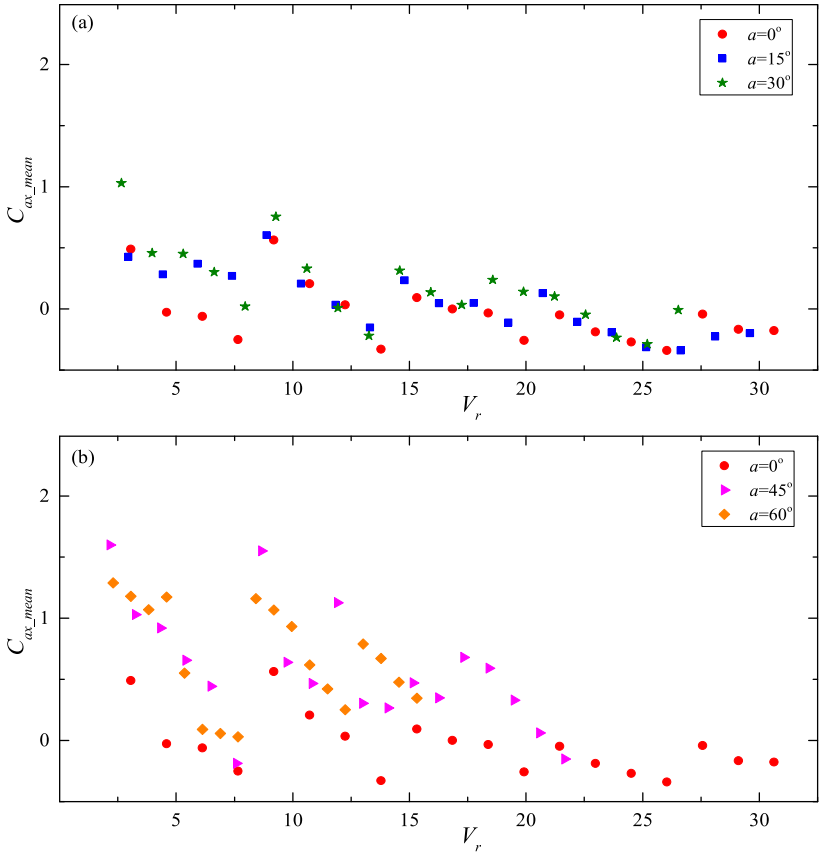

Fig. 14. Axial mean added mass coefficients in the IL direction versus the reduced velocity. (a) $a = 0°$, 15° and 30°; (b) $a = 0°$, 45° and 60°.

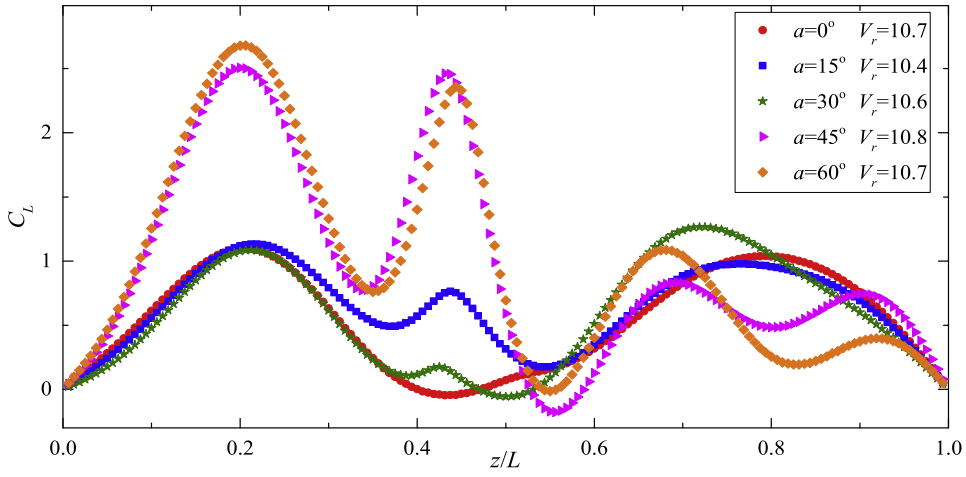

Fig. 15. Axial distribution of lift coefficients of the inclined flexible cylinder at the 2nd mode resonance.

and 60° are similar to each other and both of them are significantly different from that of the vertical flexible cylinder. It can be concluded that the axial distribution of the lift coefficient of the inclined flexible cylinder and the vertical flexible cylinder may differ from each other even when the dominant modes of vibration are the same. With the increase of the inclination angle, the discrepancy is enlarged.

The axial distribution of CF added mass coefficient of the inclined flexible cylinder at the 2nd mode resonance is shown in Fig. 16. It can be seen that both the inclined flexible cylinder and the vertical flexible cylinder experience a sudden change in the CF added mass coefficient around $z/L = 0.5$. However, the inclined flexible cylinder suffers a sharper variation than the vertical one. Moreover, the axial distribution of the CF added mass coefficient of the inclined flexible cylinder at different inclination angles shares a similar trend, which is different from that of the vertical flexible cylinder. For $a = 15°$ and 30°, the axial distributions of the CF added mass coefficient are close to each other. While the variation of the CF added mass coefficient along the span at $a = 45°$ is almost the same as that in the case of $a = 60°$.

Figs. 17 and 18 show the variation of varying drag and IL added mass coefficients along the structural axis at the 3rd mode resonance, respectively. It can be seen that the varying drag coefficient of the inclined

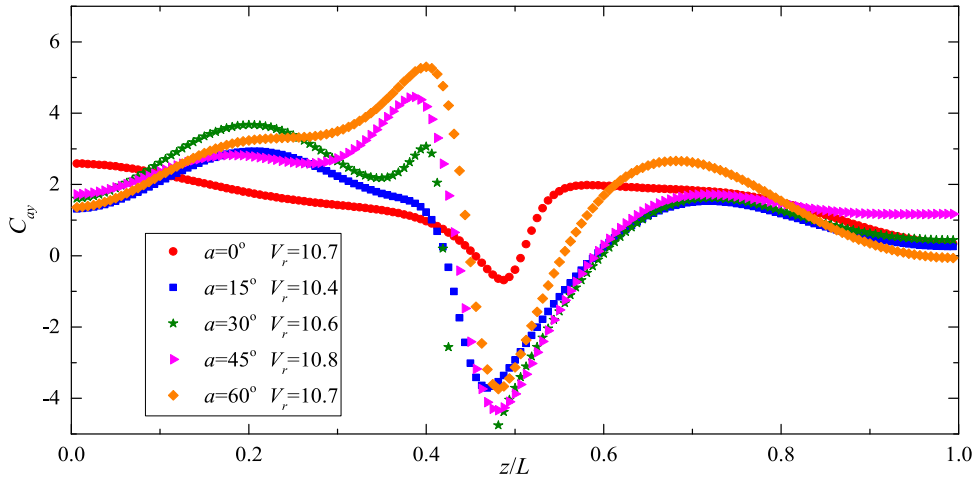

Fig. 16. Axial distribution of CF added mass coefficients of the inclined flexible cylinder at the 2nd mode resonance.

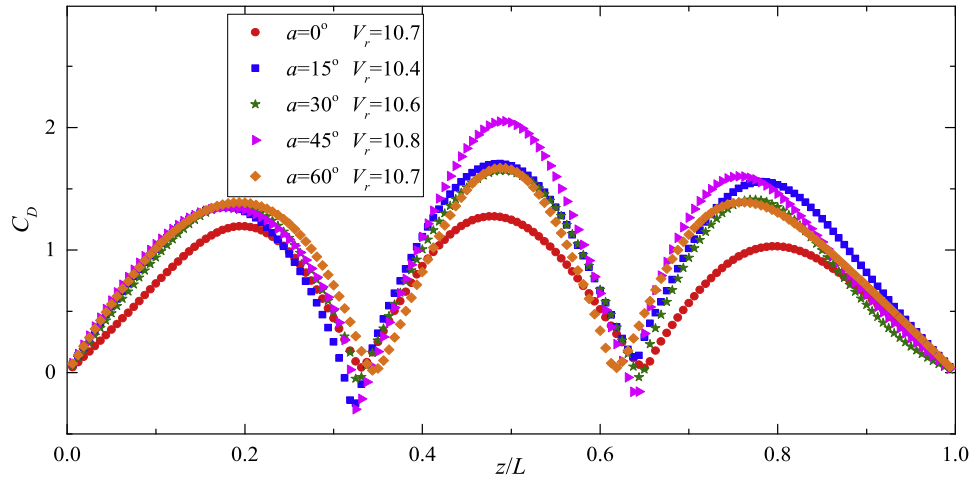

Fig. 17. Axial distribution of varying drag coefficients of the inclined flexible cylinder at the 3rd mode resonance.

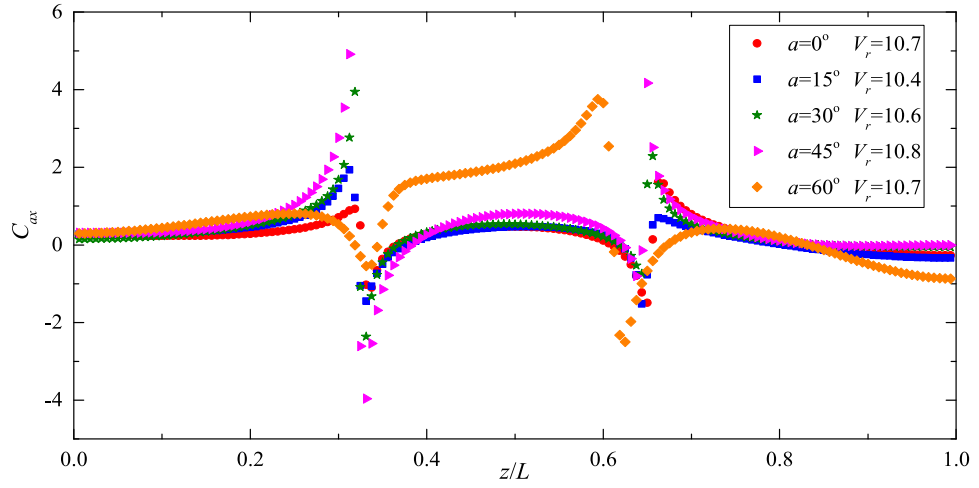

Fig. 18. Axial distribution of IL added mass coefficients of the inclined flexible cylinder at the 3rd mode resonance.

flexible cylinder and the vertical one have identical spanwise evolution, despite higher values are observed for the inclined flexible cylinder. The axial distributions of the varying drag coefficients of the inclined flexible cylinder at different inclination angles agree well with each other. For $a \leq 45^{\circ}$, the axial distribution of the IL added mass coefficient agrees well with that of the vertical flexible cylinder. The IL added mass coefficient in the case of $a = 60^{\circ}$ is close to that in the normal case in the ranges of $z/L \leq 0.3$ and $z/L \geq 0.7$. In contrast, the IL added mass coefficient of the inclined cylinder is much higher than that of the vertical one in the range of $0.35 \leq z/L \leq 0.60$.

5. Conclusions

The hydrodynamic coefficients of the inclined flexible cylinder undergoing VIV were indirectly obtained by an inverse method using the displacement responses from the model tests. The hydrodynamic features were presented and discussed. Following conclusions can be drawn.

(1) The effects of inclination angle on the RMS of the CF and IL fluctuating force coefficients (C_{CF_rms} and C_{IL_rms}) are insignificant for $\alpha = 15^\circ$. The C_{CF_rms} in the cases of $\alpha = 45^\circ$ and 60° are enlarged at the 1st and 2nd mode resonance. The C_{IL_rms} at $\alpha = 45^\circ$ and 60° shows obvious disparity from that in the normal case. For $\alpha = 60^\circ$, the peak values of the C_{IL_rms} surpass that of the vertical one. A similar upward trend of fluctuating force coefficients in the CF and IL directions for $\alpha = 60^\circ$ was also reported in Bourguet et al. [27], which might be attributed to the considerable influence of the part of the axial flow component perpendicular to the cylinder.

(2) The mean drag coefficients (C_{D0}) are positively related to the CF displacements, which is consistent with the previous results [10,15,26]. The C_{D0} show unremarkable reduction with the increase of the inclination angles, which conflicts with the experimental results of the rigid cylinder [26]. In the case of $\alpha = 60^\circ$, the C_{D0} are significantly higher than the normal case. The enlargement of C_{D0} on an elastically supported rigid cylinder inclined at 45° and a flexible cylinder inclined at 80° has been numerically observed by Zhao et al. [23] and Bourguet and Triantafyllou [28].

(3) The discrepancy of the axial mean lift and varying drag coefficients between the inclined flexible cylinder and the vertical one is enhanced as the increase of inclination angle. The peaks of the axial mean lift coefficients in the cases of $\alpha = 45^\circ$ and 60° are outstanding compared to that of the vertical one. The variation of the axial mean varying drag coefficients in the cases of $\alpha = 45^\circ$ and 60° are remarkably different from that in the normal case. Although flow structures behind the flexible cylinder in the current research are unknown, we can still deduce that the difference in the lift and varying drag coefficients of the inclined flexible cylinder is primarily due to the distinctive wake patterns according to the previous research about the wake patterns downstream an inclined cylinder through experimental [21] or numerical studies [22–24,27,28,35,36].

(4) The influences of the inclination angle on the axial mean added mass coefficients are mild in cases of $\alpha \leq 30^\circ$. At $\alpha = 45^\circ$ and 60°, the IL added mass coefficients are much larger than those at the other inclination angles. It must be pointed out that the added mass coefficients in the cases of $\alpha = 30^\circ$ and 45° surpass that in the other cases when the reduced velocity is roughly in the range of 17.0–20.0, which is due to the fact that the vibration of flexible cylinder enters the next dominant mode earlier.

(5) Within the same mode synchronized region, the spanwise evolutions of hydrodynamic coefficients in the cases of $\alpha \leq 30^\circ$ share a similar trend. However, the axial distributions of the hydrodynamic coefficients of the inclined flexible cylinder at $\alpha = 45^\circ$ and 60° are close to each other.

Acknowledgment

This research work was finically supported by National Natural Science Foundation of China (Grants Nos. 51479135, 51679167 and 51525803).

References

[1] Williamson CHK, Govardhan R. A brief review of recent results in vortex-induced vibrations. J Wind Eng Ind Aerodyn 2008;96:713–35.
[2] Bearman PW. Circular cylinder wakes and vortex-induced vibrations. J Fluids Struct 2011;27:648–58.
[3] Postnikov A, Pavlovskaia E, Wiercigroch M. 2DOF CFD calibrated wake oscillator model to investigate vortex-induced vibrations. Int J Mech Sci 2017;127:176–90.
[4] Gabbai RD, Benaroya H. An overview of modeling and experiments of vortex-induced vibration of circular cylinders. J Sound Vib 2005;282:575–616.
[5] Pavlovskaia E, Keber M, Postnikov A, Reddington K, Wiercigroch M. Multi–modes approach to modelling of vortex-induced vibration. Int J Non Linear Mech 2016;80:40–51.
[6] Bishop RED, Hassan AY. The lift and drag forces on a circular cylinder in a flowing fluid. Proc R Soc Lond 1964;277(1368):32–50.
[7] Norberg C. Fluctuating lift on a circular cylinder: review and new measurements. J Fluids Struct 2003;17:57–96.
[8] Gopalkrishnan R. Vortex induced forces on oscillating bluff cylinders. Massachusetts Institute of Technology; 1993.
[9] Aronsen KH. An experimental investigation of in-line and combined in-line and cross-flow vortex induced vibrations. Norwegian University of Science and Technology; 2007.
[10] Jauvtis N,, Williamson CHK. The effect of two degrees of freedom on vortex-induced vibration at low mass and damping. J Fluid Mech 2004;509:23–62.
[11] Vikestad K,, Vandiver JK, Larsen CM. Added mass and oscillation frequency for a circular cylinder subjected to vortex-induced vibrations and external disturbance. J Fluids Struct 2000;14:1071–88.
[12] Branković M,, Bearman PW. Measurements of transverse forces on circular cylinders undergoing vortex-induced vibration. J Fluids Struct 2006;22:829–36.
[13] Sarpkaya T. Hydrodynamic damping, flow-induced oscillations, and biharmonic response. J Offshore Mech Arct Eng 1995;117:232–8.
[14] Chaplin JR, Bearman PW, Cheng Y, Fontaine E, Graham JMR, Herfjord K, et al. Blind predictions of laboratory measurements of vortex-induced vibrations of a tension riser. J Fluids Struct 2005;21:25–40.
[15] Huera-Huarte FJ. Multi-mode vortex-induced vibrations of a flexible circular cylinder. Imperial College London; 2006.
[16] Tang G, Lu L, Teng B, Park H, Song J, Zhang J. Identification of hydrodynamic coefficients from experiment of vortex-induced vibration of slender riser model. Sci China Technol Sci 2011;54:1894–905.
[17] Song L, Fu S, Cao J, Ma L, Wu J. An investigation into the hydrodynamics of a flexible riser undergoing vortex-induced vibration. J Fluids Struct 2016;63:325–50.
[18] Wu J, Lie H, Larsen CM, Liapis S, Baarholm R. Vortex-induced vibration of a flexible cylinder: interaction of the in-line and cross-flow responses. J Fluids Struct 2016;63:238–58.
[19] Hanson AR. Vortex shedding from yawed cylinders. AIAA J 1966;4:738–40.
[20] Van Atta CW. Experiments on vortex shedding from yawed circular cylinders. AIAA J 1968;6:931–3.
[21] Ramberg SE. The effects of yaw and finite length upon the vortex wakes of stationary and vibrating circular cylinders. J Fluid Mech 1983;128:81–107.
[22] Zhao M, Cheng L, Zhou T. Direct numerical simulation of three-dimensional flow past a yawed circular cylinder of infinite length. J Fluids Struct 2009;25:831–47.
[23] Zhao M, Thapa J, Cheng L, Zhou T. Three-dimensional transition of vortex shedding flow around a circular cylinder at right and oblique attacks. Phys Fluids 2013;25:477–539.
[24] Lucor D,, Karniadakis GEM. Effects of oblique inflow in vortex-induced vibrations. Flow. Turbul Combust 2003;71:375–89.
[25] Franzini GR, Fujarra ALC, Meneghini JR, Korkischko I, Franciss R. Experimental investigation of vortex-induced vibration on rigid, smooth and inclined cylinders. J Fluids Struct 2009;25:742–50.
[26] Franzini GR, Gonçalves RT, Meneghini JR, Fujarra ALC. One and two degrees-of-freedom vortex-induced vibration experiments with yawed cylinders. J Fluids Struct 2013;42:401–20.
[27] Bourguet R,, Em Karniadakis G, Triantafyllou MS. On the validity of the independence principle applied to the vortex-induced vibrations of a flexible cylinder inclined at 60°. J Fluids Struct 2015;53:58–69.
[28] Bourguet R,, Triantafyllou MS. Vortex-induced vibrations of a flexible cylinder at large inclination angle. J Fluid Mech 2016;809:111–34.
[29] Han Q, Ma Y, Xu W, Lu Y, Cheng A. Dynamic characteristics of an inclined flexible cylinder undergoing vortex-induced vibrations. J Sound Vib 2017;394:306–20.
[30] Xu W, Ma Y, Ji C, Sun C. Laboratory measurements of vortex-induced vibrations of a yawed flexible cylinder at different yaw angles. Ocean Eng 2018;154:27–42.
[31] Lie H, Kaasen KE. Modal analysis of measurements from a large-scale VIV model test of a riser in linearly sheared flow. J Fluids Struct 2006;22:557–75.
[32] Sanaati B,, Kato N. Vortex-induced vibration (VIV) dynamics of a tensioned flexible cylinder subjected to uniform cross-flow. J Mar Sci Technol 2013;18:247–61.
[33] Vandiver KJ. Drag coefficients of long flexible cylinders. In: Proceedings of the offshore technology conference; 1983. p. 10.
[34] Song L, Fu S, Dai S, Zhang M, Chen Y. Distribution of drag force coefficient along a flexible riser undergoing VIV in sheared flow. Ocean Eng 2016;126:1–11.
[35] Lam K, Lin YF, Zou L, Liu Y. Investigation of turbulent flow past a yawed wavy cylinder. J Fluids Struct 2010;26:1078–97.
[36] Zhao M. The validity of the independence principle applied to the vortex-induced vibration of an inclined cylinder in steady flow. Appl Ocean Res 2015;53:155–60.